# Path Loss Model for UAV-assisted RFET

Suraj Suman, Sidharth Kumar, and Swades De, *Senior Member, IEEE*

***Abstract*—In this paper, we develop channel models for unmanned aerial vehicle (UAV) aided air-to-ground (AtG) radio frequency energy transfer (RFET). AtG path loss plays a key role in RFET-based recharging of field nodes. Representative field environments consist of different types of built-up areas, namely, suburban, urban, dense urban, urban high-rise, and rural agriculture deployment scenarios. For emulating the built-up areas, ITU-R recommendations are considered, whereas for rural agricultural field deployment scenario, dynamics of vegetation growth with time is considered. Accuracy of the proposed path loss models are validated by conducting real AtG RF transmission experiments in emulated suburban and agricultural fields.**

***Index Terms*—Unmanned aerial vehicle, RF energy transfer, air-to-ground path loss, modeling, wireless sensor network**

## I. Introduction

Unmanned aerial vehicle (UAV) is a programmable aircraft that can carry camera, sensor, communication equipment or other payloads to complete arduous task that is otherwise difficult for human intervention. The possible use cases include monitoring and survey, agriculture, defense, logistics, and wireless access [1]. Excellent maneuvering capability, programming flexibility, controlled access from remote place, lightweight, and low cost are the key enablers of UAV utility.

Among the emerging UAV applications, energy replenishment to wireless sensor network (WSN) is expected to be one. WSN is an integral part of internet of things (IoT), as it connects real world to the digital world for monitoring, actuation, and control. Most of these sensor nodes consume appreciable energy, which is supplied by batteries having limited lifetime. Battery replacement is neither cost-effective nor feasible in many cases. This can be overcome by charging wirelessly from a power source. Magnetic resonance coupling based power transfer from UAV is studied in [2]. But due to vibration, misalignment of coils, and deformation in coils, the performance can be very poor. For uninterrupted network operation, energy supply via radio frequency energy transfer (RFET) is a promising technique, where the issues of misalignment, vibration, etc. have much less detrimental effects on performance [3]. Recharging time of a node strongly depends on the harvested power by RFET, which relies on received power and is determined by path loss. Therefore, to be able to accurately estimate the charging time via air-to-ground (AtG) RFET, it is important to develop an accurate path loss model.

*1) Related Work and Motivation:* Path loss models for some AtG signal propagation scenarios for relatively long range communications have been reported in literature. Elevation angle dependent model is presented in [4], [5] for suburban, urban, dense urban areas, and high-rise buildings. AtG channel is also investigated for over-water, hilly, and mountainous areas [6], [7]. Stochastic channel model with only line-of-sight (LoS) communication is studied in [8].

The works on UAV channel analysis focus on High Altitude Platform having deployment height on the order of kilometers [4], [6], [7] or Low Altitude Platform having deployment height around 100 m [5]. These models are useful for cellular communications, where the transmitter-receiver pairs are separated by a large distance. Hence, the scatterer and reflector heights are typically less than the deployment height of UAV.

Due to low sensitivity and poor rectification efficiency at low received power, RFET requires very low deployment altitude, about a few meters [9]. In such a scenario, height of the scatterers could be mostly higher than the UAV deployment altitude. This distinct deployment conditions motivate us to freshly investigate the path loss and shadowing statistics in UAV-assisted RFET to field nodes. Note that, unlike in data communications, where multipath fading plays a key role [10], due to longer time scale of RFET operation, the effect of shadowing is more prominent in UAV-assisted RFET.

*2) Contribution and Scope:* The key features and novelty of our work are as follows: (1) Urban/suburban as well as agricultural deployment specific simulation of AtG RFET are conducted using a wireless propagation software, and the corresponding path loss models are developed and parameters are estimated. (2) Plant growth dynamics with time is considered to emulate rural agriculture field environment. (3) Accuracy of the AtG RFET channel models are verified by conducting extensive field measurements, which was not done before.

Now-a-days, automation is being augmented to IoT-enabled WSNs for field data collection and message exchange, where online recharging is important. Advancements in miniature aircraft technology [11] is an enabler to UAV-aided recharging, where the proposed AtG path loss models are useful.

## II. Urban/Suburban Environments

Emulation of a deployment area is challenging, as huge variation is observed in real-life. Here, International Telecommunication Union Radiocommunication (ITU-R) recommendations are used to realize a urban/suburban scenario [12].

*1) Deployment Layout:* A typical suburban scenario contains approximately $10\%$ build-up area, 750 buildings per unit area, and the building heights follow Rayleigh distribution with mean building height $8$ m. With these considerations, layout of a deployment area for analysis is shown in Fig. 1(a). Concrete material is considered as the outer layer of building, whereas the ground is dry earth. Wireless InSite propagation software [13] is used to simulate the ray propagation between

This work has been supported by the Department of Telecom. under the grant for building end to end 5G test-bed, along with the Department of Electron. and Inform. Technol. under Visvesvaraya PhD Fellowship scheme.

The authors are with the Department of Electrical Eng. and Bharti School of Telecom, Indian Institute of Technology Delhi, New Delhi, India (e-mail: {suraj.suman, sidharth.kumar, swadesd}@ee.iitd.ac.in)

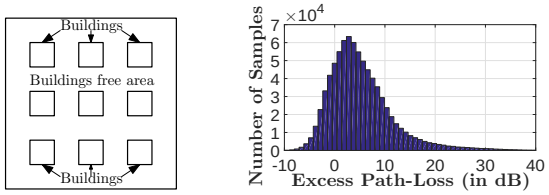


(a) (b)

**Figure 1:** (a) Suburban layout; (b) histogram of excess path loss.

transmitter and receiver. Here, during signal propagation four types of rays are accounted: *direct, diffracted, reflected*, and *transmitted*. The resultant electric field is the vector sum of all the electric fields. The isotropic transmitter transmits 0 dBm power. The receiver with isotropic antenna was placed on ground, each position separated from other by distance 0.5 m. Transmitting and receiving antenna were with vertical polarization. Path loss is measured at each receiver by placing the transmitter at different heights: 1 to 10 m above ground.

*2) Channel Modeling:* Path loss at the $k^{\text{th}}$ position is:

$$PL_k^{cal} = 10\log_{10}(P_{tx}) - 10\log_{10}(P_{rx_k}) \quad [\text{in dB}] \quad (1)$$

where $P_{tx}$ is the power transmitted by transmitter mounted on UAV and $P_{rx_k}$ is the received power at the $k^{\text{th}}$ position.

Excess path loss at the $k^{\text{th}}$ position ($\mathcal{X}_k$) is defined as:

$$\mathcal{X}_k \triangleq PL_k^{cal} - PL_k^{fs} \qquad [\text{in dB}]. \quad (2)$$

$PL_k^{cal}$ is calculated from simulation, whereas $PL_k^{fs}$ is the free space path loss obtained from Friis equation, given as:

$$PL_k^{fs} = 20\log_{10}(l_k) + 20\log_{10}(4\pi f/c). \quad (3)$$

$l_k$ is the distance between transmitter and $k^{\text{th}}$ receiver position, $f$ is signal frequency, and $c$ is speed of light. Total path loss can be thought as sum of free space loss and excess loss, which is studied here via analytical modeling as well as field measurements. Friis equation gives free space path loss at a given location; we have to model the excess path loss only.

At $f = 915$ MHz and with UAV altitude 2 m, excess path loss in Fig.1(b) indicates a single group of propagation, which is in contrast with the path loss model proposed for aerial communication [4], [5]. The propagation trait strongly depends on transmitter height from the field nodes, obstruction heights, and their relative separation. In UAV-assisted RFET, the operational altitude being very low, transmitter-receiver distance is small, resulting in non-severe signal attenuation.

We now model the excess path loss. Unlike in terrestrial cellular networks where the BS height is fixed, in UAV-assisted AtG RFET the hovering altitude and position changes with respect to the sensors located on the ground. Since shadowing statistics changes significantly with UAV altitude variation, in order to incorporate the varying UAV altitude in a generalized sense, excess path loss is modeled as a function of elevation angle $\theta$ which is the ratio of UAV deployment height and transmitter-receiver separation distance. Variation of cumulative distribution function (CDF) of the original and fitted data are shown in Fig. 2(a). The excess path loss for each $\theta$ is separately computed; its variation found to closely follow Normal distribution, which is modeled as:

$$\mathcal{X} \sim \mathcal{N}\Big(\mu(\theta), \sigma^2(\theta)\Big). \quad (4)$$

Based on these observations it is deduced that, the AtG path loss for RFET in suburban environments can be modeled as single group of propagation using Normal distribution.

The mean (in dB) and variance (in dB) are found to fit as:

$$\mu(\theta) = a \cdot \exp(b \cdot \theta), \quad \sigma^2(\theta) = c \cdot \exp(d \cdot \theta) \quad (5)$$

where $a = 12.05,\ b = -0.0742,\ c = 79.24,\ d = -0.08175$. R-square values for mean and variance fitting are respectively 0.9893 and 0.9705, which are within the acceptable range of goodness of fit [14]. Figs. 2(b) and 2(c) show the variation of original and fitted mean and variance against the elevation angle. Observe that, at higher elevation angles the shadowing loss is less because the distance is less and lesser number of obstructions appear. At lower elevation angles, the signal suffers more severely as more obstructions appear in the path.

For comparison, mean and variance of received signal using the models in [4] and [5] are also plotted. Root mean square error (RMSE) of mean and variance of the proposed model are respectively 0.29 dB and 2.83 dB, whereas the RMSE reported in [4] and [5] are respectively 4.3968 dB and 2.9759 dB for mean, and respectively 9.9066 dB and 29.5187 dB for variance. Such huge difference in path loss with the existing models corroborates importance of the proposed model.

*3) Experimental Validation:* To verify correctness of the fitted model, field experiments were conducted in an underground parking lot, where long and wide pillars emulate buildings in suburban scenario. Fig. 2(d) shows the setup with adjustable altitude for UAV-aided RFET. Powercast TX91501 transmitter (www.powercastco.com) was used as RF source; N9918A spectrum analyzer captured received signal power. The received power were recorded for different heights and radial distances to emulate distinct elevation angles of the UAV. As shown in Figs. 2(b), and 2(c), mean and variance of excess path loss from experiments closely match the simulation results; the relative errors are respectively 5.44 % and 7.08 %, which are within the acceptable statistical limit [15].

Similarly, modeling in three other environments, urban, dense urban, and high-rise urban, were conducted to cover a wide range of possible deployments. The empirical parameter values for excess path loss in all four environments are listed in Table I. Next, we consider modeling in agricultural field, having the unique features of vegetation growth.

**Table I:** Values of empirical parameters of excess path loss.

| **Environment** | $a$ | $b$ | $c$ | $d$ |
|---|---|---|---|---|
| Suburban | 12.05 | $-0.0742$ | 79.24 | $-0.0817$ |
| Urban | 22.09 | $-0.0430$ | 652.47 | $-0.1037$ |
| Dense urban | 28.74 | $-0.0558$ | 702.23 | $-0.0782$ |
| High-rise urban | 46.39 | $-0.0482$ | 806.21 | $-0.0384$ |

## III. Agriculture Environment

Agricultural plant growth is expected to have strong impact on path loss. So, this growth dynamics must be incorporated in the model. In order to capture this variation, in simulations rice plant is considered which grows fast until ripening.

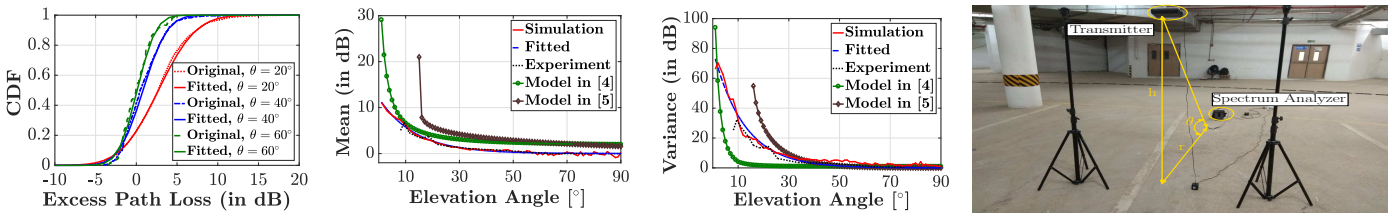


(a) CDF (b) Mean (c) Variance (d) Experimental set up

**Figure 2:** (a) CDF of excess path loss at different elevation angle; variation of original, fitted, and experimental values of (b) mean and (c) variance against elevation angle for suburban environment; (d) experimental set up.

*1) Deployment Layout:* Using the data in [16], plant growth dynamics is closely approximated using sigmoid function as:

$$H_P(t) = \frac{95.45}{1+\exp(-0.068(t-26.65))}, \quad 0 \le t \le 70 \quad (6)$$

where $H_P(t)$ (in cm) is the plant height after $t$ days of sowing.

Factors that affect the RF signal propagation through foliage are dimension and density of plant leaves. Time-varying density of leaves $\rho_P(t)$ is modeled as:

$$\rho_P(t) = \frac{n_P \times L_P(t)}{A \times H_P(t)} \quad (7)$$

where $n_P$ is the total number of plants in a given area Area $A$, $L_P(t)$ is the number of leaves per plant after $t$ days of sowing. For maximum yield of rice cultivation, plantation is done with inter-plant separation 20 cm [17]. The data on leaf dimension and number of leaves per plant are taken from [18].

Layout of $100\times100$ m$^2$ area (cf. Fig. 3(a)) is considered for simulation using Wireless InSite software. A plant block area is $5\times5$ m$^2$, and the inter-block spacing is 0.5 m. Transmitter height is varied from 1 m to 10 m. The nodes are considered placed on ground with 0.5 m spacing from each other.

*2) Channel Modeling:* Like in urban/suburban scenario, we model the excess path loss for different elevation angles and plant heights. Assuming all plants have same height at time $t$, the excess loss at $k^{\text{th}}$ position with plant height $H_P(t)$ is:

$$\mathcal{X}_k(H_P(t)) = PL_k^{cal}(H_P(t)) - PL_k^{fs} \quad \text{[in dB]} \quad (8)$$

where $PL_k^{cal}(H_P(t))$ is the path loss calculated from simulation and $PL_k^{fs}$ is free space path loss, calculated using (3).

The histogram of excess path loss, when UAV hovers at height 2 m, is shown in Fig. 3(b)-(d) for different plant heights, which indicates two groups of propagation. The portion of histogram situated at lesser path loss points to LoS communication, whereas the other having higher path loss points to non-LoS (NLoS) communication. This occurs because in the considered deployment scenario the transmitter mounted on UAV is always above the shadowing elements, i.e., the plants.

These two groups (LoS and NLoS) need to be modeled separately. Therefore, the excess path loss is classified in two groups using K-means clustering for a given plant height. For each group of propagation (LoS and NLoS), the data for each elevation angle is analyzed separately. It is observed that, for a given plant height the excess path loss closely follows Normal distribution at different elevation angles. After fitting these data to each plant height, the variation of excess path loss with plant height and elevation angle can be modeled as:

$$\mathcal{X}(H_P(t)) \sim \begin{cases} \mathcal{N}\Big(\mu_1(H_P(t),\theta), \sigma_1^2(H_P(t),\theta)\Big), \text{LoS} \\ \mathcal{N}\Big(\mu_2(H_P(t),\theta), \sigma_2^2(H_P(t),\theta)\Big), \text{NLoS} \end{cases} \quad (9)$$

where $\mu_1(\theta, H_P(t))$ and $\sigma_1^2(\theta, H_P(t))$ are respectively mean and variance of LoS component, which are obtained as:

$$\mu_1(H_P(t),\theta) = \alpha\theta^\beta + \gamma, \quad \sigma_1^2(H_P(t),\theta) = \delta\theta^\zeta \quad (10)$$

$$\text{with } \alpha = 141.3\exp\Big[-\Big(\frac{H_P(t)-74.98}{24.98}\Big)^2\Big],\ \beta = 0.95,$$
$$\gamma = -2.123\exp\Big[-\Big(\frac{H_P(t)-74.72}{23.76}\Big)^2\Big],$$
$$\delta = 209.8\exp\Big[-\Big(\frac{H_P(t)-74.65}{18.57}\Big)^2\Big],$$
$$\zeta = -1.339\exp\Big[-\Big(\frac{H_P(t)-85.31}{84.97}\Big)^2\Big].$$

R-square values for fitting of $\alpha, \gamma, \delta$, and $\zeta$ are respectively 0.9533, 0.9171, 0.9942, and 0.9537. $\mu_2(H_P(t),\theta)$ and $\sigma_2^2(H_P(t),\theta)$ are mean and variance of NLoS component with plant height $H_P(t)$ and elevation angle $\theta$. They are found as:

$$\mu_2(H_P(t),\theta) = \phi\exp(\psi\cdot\theta), \quad \sigma_2^2(H_P(t),\theta) = \Phi\theta^\Psi \quad (11)$$

$$\text{where } \phi = -0.06765H_P^2(t) + 5.4139H_P(t) - 49.49,$$
$$\psi = 0.000148H_P^2(t) - 0.007299H_P(t) + 0.02134,$$
$$\Phi = -2.567H_P^2(t) + 147.2H_P(t) - 1399,$$
$$\Psi = 0.0003611H_P^2(t) - 0.01388H_P(t) - 0.2281.$$

The R-square values for fitting of $\phi, \psi, \Phi$, and $\Psi$ are respectively 0.9879, 0.9942, 0.9669, and 0.9905.

The LoS probability $p_{LoS}(H_P(t),\theta)$ for different plant height and elevation angle is modeled as:

$$p_{LoS}(H_P(t),\theta) = \begin{cases} u_1\theta + u_2 & \text{if } \theta^\circ < 4 \\ v_1\theta^3 + v_2\theta^2 + v_3\theta + v_4 & \text{if } 4 \le \theta^\circ \le 16 \\ 1 & \text{if } 16 < \theta^\circ \end{cases}$$

with $u_1, u_2, v_1, v_2, v_3$, and $v_4$ in (12), the respective R-square values for fitting are 0.9513, 0.9531, 0.9905, 0.9629, 0.9875, 0.9951, and 0.9403. The probability of NLoS group of propagation is: $p_{NloS}(H_P(t),\theta) = 1 - p_{LoS}(H_P(t),\theta)$.

Variation of mean and variance for different plant heights are shown in Figs. 4(a) and 4(b). It is observed that excess path loss increases with growth of plant height, because attenuation rate as well as scattering dominate at higher plant height.

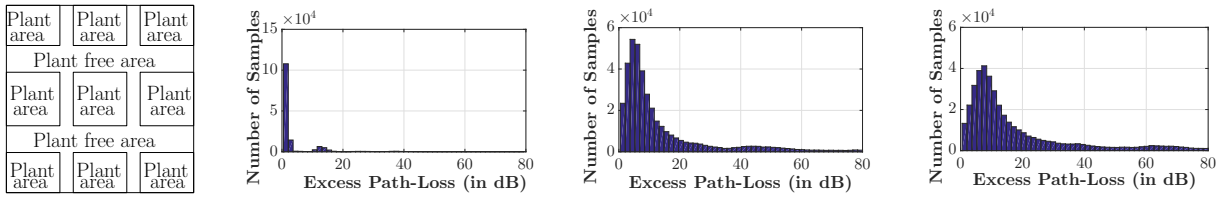


(a) (b) $H_P = 30$ cm (c) $H_P = 50$ cm (d) $H_P = 90$ cm

**Figure 3:** (a) Agricultural field layout; histogram of excess path loss for plant heights (b) 30 cm, (c) 50 cm, and (d) 90 cm.

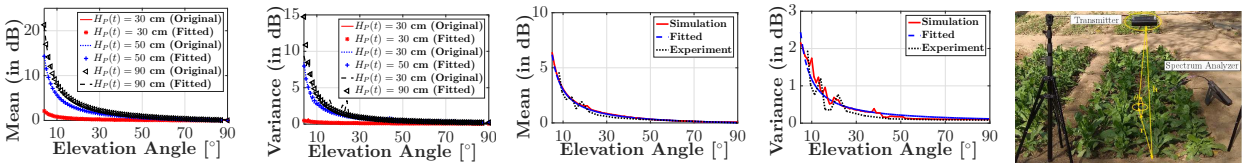


(a) Mean (b) Variance (c) $H_p = 37$ cm (d) $H_p = 37$ cm (e) Experimental set up

**Figure 4:** Experimental validation of the proposed path loss model in agricultural scenario.

$$u_1 = 0.1825 = 0.1387\cos\left(\frac{\theta}{7.47}\right) + 0.1114\sin\left(\frac{\theta}{7.47}\right), u_2 = 70.18\exp\left[-\left(\frac{\theta-25}{2.422}\right)^2\right],$$
$$v_1 = \frac{1}{382.4}\exp\left[-\left(\frac{\theta-79.21}{7.579}\right)^2\right],\ v_2 = \frac{1}{11.84}\exp\left[-\left(\frac{\theta-79.12}{6.52}\right)^2\right],\ v_3 = \frac{1}{1.18}\exp\left[-\left(\frac{\theta-79.1}{6.21}\right)^2\right], \quad (12)$$
$$v_4 = 0.9056 - 0.1609\cos\left(\frac{\theta}{12.05}\right) + 0.1411\sin\left(\frac{\theta}{12.05}\right).$$

*3) Experimental Validation:* The experimental setup for agricultural scenario is shown in Fig. 4(e); the same equipments were used as in suburban setting. A plant nursery with plantation height about 37 cm was used for conducting the experiments. Good match with the simulated values are observed (cf. Fig. 4(c) and (d)). The relative error for mean and variance are 3.44 % and 6.48 %, respectively, which validate the proposed path loss model. We believe, approximations in Wireless InSite propagation software with respect to the actual plantation setting are the major reasons for the relative error.

## IV. Concluding Remarks

This paper has presented excess path loss models for UAV-assisted AtG RFET in urban/suburban and agricultural deployments. The modelings have been performed by conducting environment specific simulation using a standard wireless propagation software, where elevation angle has been used to model the shadow statistics. Single group of propagation has been observed in urban/suburban scenarios, whereas two group of propagation have been observed in agricultural environment. Accuracy of the proposed models have been verified by field experiments and extensive measurements.

Total path loss at a receiver is: $PL = PL^{fs} + \mathcal{X}$. $PL^{fs}$ denotes free space path loss, given in (3); $\mathcal{X}$ denotes excess path loss, obtained from the developed expressions in (4) for urban/suburban setting, and (9) for agricultural environment.

## References


[1] Y. Zeng *et al.*, "Wireless communications with unmanned aerial vehicles: opportunities and challenges," *IEEE Commun. Mag.*, vol. 54, May 2016.

[2] B. Griffin and C. Detweiler, "Resonant wireless power transfer to ground sensors from a UAV," in *Proc. IEEE Int. Conf. Robot. and Autom.*, 2012.

[3] X. Mou and H. Sun, "Wireless power transfer: Survey and roadmap," in *Proc. IEEE VTC (Spring)*, May 2015, pp. 1–5.

[4] J. Holis and P. Pechac, "Elevation dependent shadowing model for mobile communications via high altitude platforms in built-up areas," *IEEE Trans. Antennas Propag.*, vol. 56, pp. 1078–1084, Apr. 2008.

[5] A. Al-Hourani *et al.*, "Modeling air-to-ground path loss for low altitude platforms in urban environments," in *Proc. IEEE GLOBECOM*, 2014.

[6] R. Sun and D. W. Matolak, "Air-ground channel characterization for unmanned aircraft systems- part II: Hilly and mountainous settings," *IEEE Trans. Veh. Technol.*, vol. 66, no. 3, pp. 1913–1925, Mar. 2017.

[7] D. W. Matolak and R. Sun, "Air-ground channel characterization for unmanned aircraft systems- part I: Methods, measurements, and models for over-water settings," *IEEE Trans. Veh. Technol.*, vol. 66, 2017.

[8] W. Khawaja *et al.*, "UWB channel sounding and modeling for UAV air-to-ground propagation channels," in *Proc. IEEE GLOBECOM*, 2016.

[9] S. Suman *et al.*, "UAV-assisted RF energy transfer," in *Proc. IEEE ICC*, May 2018, pp. 1–6.

[10] M. M. Azari *et al.*, "Ultra reliable UAV communication using altitude and cooperation diversity," *IEEE Trans. Commun.*, vol. 66, 2018.

[11] D. Floreano and R. J. Wood, "Science, technology and the future of small autonomous drones," *Nature*, vol. 521, no. 7553, May 2015.

[12] "Propagation data and prediction methods for the planning of short-range outdoor radiocommunication systems and radio local area networks in the frequency range 300 MHz to 100 GHz," Rec. ITU-R P.1411-9, 2017.

[13] Wireless InSite. [Online]. Available: https://www.remcom.com/wireless-insite-em-propagation-software/.

[14] D. Hooper *et al.*, "Structural equation modelling: Guidelines for determining model fit," *Electron. J. Bus. Res. Methods*, vol. 6, Jan. 2008.

[15] H. Park and L. A. Stefanski, "Relative-error prediction," *Statistics & probability Lett.*, vol. 40, no. 3, pp. 227–236, Oct. 1998.

[16] A. Kotera and E. Nawata, "Role of plant height in the submergence tolerance of rice: a simulation analysis using an empirical model," *Agricultural Water Management*, vol. 89, no. 1, pp. 49–58, Apr. 2007.

[17] K.-I. Hibara *et al.*, "Jasmonate regulates juvenile-to-adult phase transition in rice," *Development*, vol. 143, no. 18, pp. 3407–3416, Sept. 2016.

[18] Y. Zhu *et al.*, "Modelling leaf shape dynamics in rice," *NJAS-Wageningen J. Life Sci.*, vol. 57, no. 1, pp. 73–81, Dec. 2009.